Initial Feasibility Study for Transurethral Kidney Surgery using a Tubular Continuum Manipulator

M. Bormann[1], J.Granna[1], F. Imkamp[2], and J. Burgner-Kahrs[1]

[1] *Leibniz Universität Hannover, Laboratory for Continuum Robotics, Hanover, Germany*
[2] *Hannover Medical School (MHH), Clinic for Urology and Urologic Oncology, Hanover, Germany*

Contact: granna@lkr.uni-hannover.de

Abstract:

Transurethral access to the kidney is mostly utilized to perform endoscopy for diagnostics and stone removal. This minimally invasive procedure is challenging, especially for those patients whose kidney branches out into fine structures. Often, existing flexible instruments are lacking manipulability, robustness, and the field of view is limited. In order to improve those aspects, we propose a new concept for transurethral kidney interventions using a tubular continuum manipulator composed of three tubes, each of which can be mechanically translated and rotated, enabling the manipulator to follow nonlinear paths. To prove our concept, an optimization algorithm is presented, which utilizes multiobjective particle swarm optimization and optimizes tube parameters for successively used sets of tubes for three specific patient kidney datasets. We further evaluate, whether sets of tubes can be determined to provide all three kidneys.

Keywords: tubular continuum manipulators, robot assisted surgery, minimally invasive surgery, transurethral surgery

1 Problem

Transurethral procedures are minimally invasive and advantageous compared to open surgery. Besides cosmetic aspects-blood loss, postoperative pain and hospitalization are reduced, while recovery from surgery is faster. Transurethral retrograde kidney endoscopy can be conducted for diagnostic or treatment reasons. Kidney stone removal is the most frequent retrograde intrarenal surgery. Generally flexible instruments (ureterorenoscope) are inserted over a guide wire into the upper urinary tract [1]. The kidney's anatomy itself is highly complex and variable, as it branches out into several chambers called renal calyces and it differs significantly from patient to patient (see Figure 1). During intervention, the instrument, consisting of at least one working channel, an optical camera and light source unit, is directed into all renal calyces, which is a complex task [1]. To obtain information about the current position of the endoscope within the urinary system and ensure that each calix has been monitored, intraoperative fluoroscopy with contrast media is widely used. The accessibility of renal calyces can be challenging, when the branches are only accessible on highly tortuous paths. In contrast to existing advantages of this procedure, intervention cost is high and robustness, especially of the ureterorenoscope is low. Further, the intervention requires experienced surgeons [2], as manipulation within the kidney is challenging due to the complex anatomy of the urinary system and difficult manual actuation of existing endoscopes.

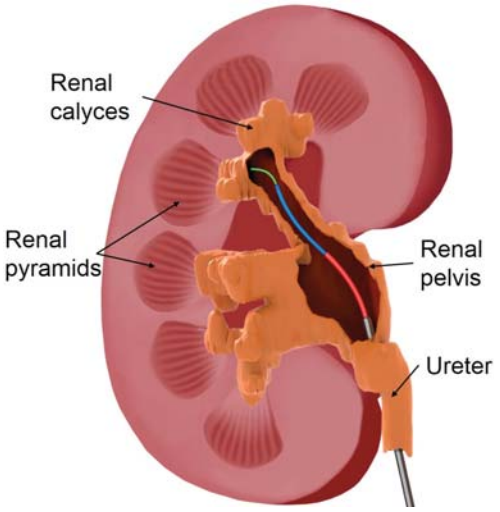

Figure 1: Tubular Manipulator composed of three tubes (red, blue, green) within the kidney extending out of an endoscope (gray).

To overcome these disadvantages, this paper presents a new concept for transurethral kidney procedures, where a tubular continuum manipulator is used to replace the ureterorenoscope. Tubular continuum manipulators enable minimally invasive surgery in hardly accessible regions [3]. They are composed of several precurved tubes inserted into one other, each of which can be actuated by translation and slight axial rotation. Our vision is that a tubular continuum manipulator consisting of three tubes is incorporated into the existing rigid endoscope, which delivers the manipulator on a straight path towards the kidney. The manipulator, its inner lumen carrying a camera, is then extended into the renal calyces by teleoperation. To the best of our knowledge, there

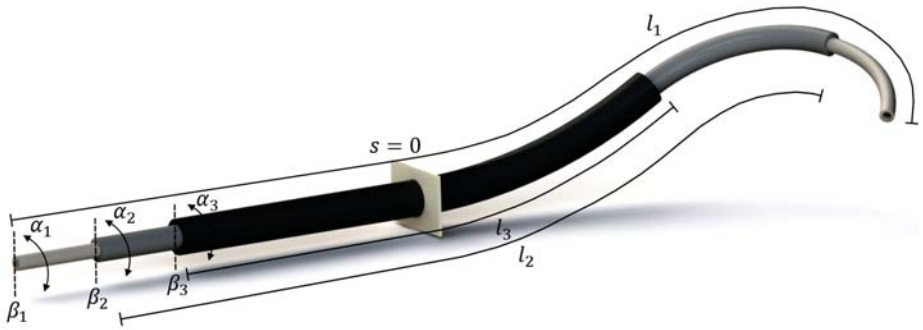

Figure 2: Tubular continuum manipulator composed of three tubes with tube length l_1, l_2, l_3, translational parameters $\beta_1, \beta_2, \beta_3$ and rotational parameters $\alpha_1, \alpha_2, \alpha_3$.

exists no robotic system until now which considers transurethral access to the kidney. However, continuum robots have been proposed for transurethral prostate surgery (e.g. [4]).

To design a tubular continuum manipulator for a specific surgical task, the design and configuration parameters have to be optimized according to specific design and anatomical constraints. As the design parameter space is diverse, researchers proposed the use of optimization algorithms, such as [5, 6, 7, 8]. However, most of these algorithms only consider non-linear optimization algorithms with one scalar error metric to be maximized or minimized. None of the existing algorithms considers multiple objectives, or consider a pareto-optimal set of solutions. However, in many surgical applications exist competing objectives such that a single error metric cannot sufficiently reflect the complexity.

Thus, we propose a new optimization approach using a multiobjective particle swarm algorithm to optimize tube parameters (length and curvatures) of the tubular continuum manipulator for transurethral kidney surgery. The contributions of this paper are: 1) design constraints for the tubular manipulator, 2) workspace characterization of three patient kidneys, 3) a new optimization algorithm which utilizes particle swarm optimization and considers multiple objectives for tube parameter optimization and 4) evaluation of the proposed algorithm considering three patient kidneys.

2 Material and Methods

2.1 Tubular Continuum Manipulator

Tubular continuum manipulators are composed out of n ($n > 2$) concentric, precurved, superelastic tubes. In this paper, we consider tubes made from the shape memory alloy Nitinol (NiTi), which remains strains up to 8% without damage. The tubes are inserted into one other and mechanical translation and rotation of each tube generates a tentacle-like motion in 3D space. In this paper, $n = 3$ concentric tubes are considered. Each tube i is defined by an inner and outer diameter ID_i and OD_i, a straight length L_{si} and a curved length L_{ci} with constant curvature κ_i. The overall length of a tube is defined as: $l_i = L_{si} + L_{ci}$, where $l_1 > l_2 > l_3$ with l_1 being the innermost tube and l_3 the outermost tube.

2.1.1 Configuration Space

The configuration space of a tubular continuum manipulator is of dimension $2n$, with the rotational parameters $\alpha_i \in [-\pi, \pi)$ and translational parameters $\beta_i \in [-\ell_i, 0]$ for each tube i which are subject to

$$\beta_1 \leq ... \leq \beta_n \leq 0, \tag{1}$$

$$\ell_n + \beta_n \leq ... \leq \ell_1 + \beta_1. \tag{2}$$

The manipulator's shape is characterized by its space curve $g(s) \in SE(3)$, which is parameterized in terms of arc length s, where $s = 0$ is defined at the constrained outlet of the manipulator, as illustrated in Figure 2. The manipulator's space curve $g(s)$ and can be determined by e.g. using the forward kinematics model in [9].

2.1.2 Design Constraints

Design constraints are formulated according to the specific anatomical constraints and the diameter of the working channel of the endoscope. Prior defined tube parameters are: $ID_1 = 1\,\text{mm}$, $OD_1 = 1.2\,\text{mm}$, $ID_2 =$

1.5 mm, $OD_2 = 1.9$ mm, $ID_3 = 2.3$ mm and $OD_3 = 3$ mm. The inner tube diameter ID_1 is chosen, such that the working channel is large enough to carry tools (e.g. laser fiber) or a camera. The outer tube diameter OD_3 is set to be 3 mm such that the tubular continuum manipulator can be incorporated into existing endoscopes. The maximum curvature κ_{max} of all tubes is limited due to the existing strain limit of $\varepsilon = 8\,\%$ of Nitinol as $\kappa_{max} = 2\varepsilon \cdot (OD_i\,(1+\varepsilon))^{-1}$. Upper and lower boundaries for the straight and curved length are chosen empirically considering kidney dimensions as: $3\,\text{mm} \leq Ls_1 \leq 140\,\text{mm}$, $2\,\text{mm} \leq Ls_2 \leq 130\,\text{mm}$, $1\,\text{mm} \leq Ls_3 \leq 120\,\text{mm}$, $0\,\text{mm} \leq Lc_1, Lc_2, Lc_3 \leq 110\,\text{mm}$.

2.2 Workspace Characterization

To optimize the tubular continuum manipulator for transurethral kidney surgery, we determine the workspace of three kidneys by segmenting the kidney's volume from 3D CT images with contrast agent and converting them into a surface dataset using 3D slicer (slicer.org). The surface datasets are then converted into a volumetric representation for further processing. We compute the insertion paths into each of the renal calyces by using a thinning algorithm [10], which removes voxels from the renal pelvis and renal calyces volume model until only the skeleton is left, as depicted in Figure 3. The endoscope outlet point (marked as a green dot) and goal positions z_o for the manipulator to reach within the renal calyces (marked as blue dots) are then selected manually by the urologist.

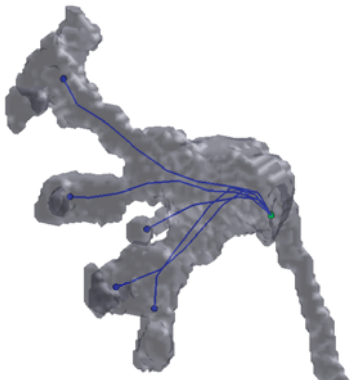

Figure 3: Renal calyces, renal pelvis and ureter in gray and insertion paths and goal positions in blue.

2.3 Tube Parameter Optimization

We use particle swarm optimization, originally published in [11], to optimize the tube parameters of the tubular continuum manipulator. The swarm or population consists of P particles. In our case, a particle $\boldsymbol{x_m}$ is defined by the tube parameters: $\boldsymbol{x_m} = [Ls_{1m}, Lc_{1m}, \kappa_{1m}, Ls_{2m}, Lc_{2m}, \kappa_{2m}, Ls_{3m}, Lc_{3m}, \kappa_{3m}]$, with $m = 1...P$. The particle $\boldsymbol{x_m}$ (which describes a solution within the search space) is defined by its current position $\boldsymbol{x_m^t}$ and moves through the search space governed by velocity $\boldsymbol{v_m^t}$ at time step t. The position and velocity of the swarm members change from generation t to generation $t+1$, where each particle's velocity $\boldsymbol{v_m^{t+1}}$ influences the particle's position $\boldsymbol{x_m^{t+1}}$ at time step $t+1$. The velocity $\boldsymbol{v_m^{t+1}}$ is governed by two guides, which are the particle's personal best solution $\boldsymbol{p_{b_m}^t}$ found so far and the global best solutions $\boldsymbol{g_{b_m}^t}$. In multiobjective particle swarm optimization [12], the quality of each particle's position is evaluated by multiple objectives. An archive $\boldsymbol{A_t}$ stores the best solutions found so far and contains the pareto-optimal solutions after the maximum number of generations has been reached. Goal of the particle swarm optimization is to find a solution for $Ls_{k_i}, Lc_{k_i}, \kappa_{k_i}$ such that a minimum number of tube sets k enable manipulation into all renal calyces of one kidney.

2.3.1 Particle Swarm Algorithm

Algorithm 1 displays the particle swarm optimization employed in this paper. Input to the algorithm is the kidney's volumetric representation and the goal positions $\boldsymbol{z_o}$ within the kidney. The algorithm is first initialized by the number of generations G, the number of particles P, the inertia coefficient w and constants c_1 and c_2, which influence the velocity $\boldsymbol{v_m^t}$ of a particle $\boldsymbol{x_m}$. Initialization of each particle's position $\boldsymbol{x_m}$, velocity $\boldsymbol{v_m}$ and archive $\boldsymbol{A_t}$ are performed. Within each generation t, each particle's cost (according to two cost functions f_1 and f_2) is determined and the archive $\boldsymbol{A_t}$ is updated. Within a population, the algorithm selects the personal $\boldsymbol{p_{b_m}}$ and global best guides $\boldsymbol{g_{b_m}}$ and updates the particle's position $\boldsymbol{x_m}$ and velocity $\boldsymbol{v_m}$ accordingly. Once the new position of a population is found, prior defined constraints on the parameter space need to be enforced. The algorithm proceeds until generation size G has been reached. Output of the algorithm are the particles (solutions) in $\boldsymbol{A_t}$. Each step is explained in the following:

Initialize: The particles $\boldsymbol{x_m}$ are initialized based on a random distribution within the parameter space. For each particle $\boldsymbol{x_m}$ the configuration space is sampled using $q = 5000$ samples to approximate the particle's coverage within the kidney. All considered samples are collision free and the manipulator's backbone remains within the kidney's volume at all times. We then determine the nearest end effector positions $\boldsymbol{ee}$ of the respective configuration samples of each particle to all goal positions $\boldsymbol{z_o}$ using the Euclidean distance. Following

Algorithm 1 MOPSO

```
INPUT: patient dataset, z_o
DEFINE G, P, w, c_1, c_2
INITIALIZE x_m, v_m, A_t
for t = 1 : G do
    {f_1, f_2} :=DETERMINE PARTICLE COST(x_m)
    A_t :=UPDATE ARCHIVE(x_m, A_{t-1}, f_1, f_2)
    for m = 1 : P do
        {p^t_{b_m}, g^t_{b_m}} :=SELECT GUIDES(A_t, x^t_m, f_1, f_2)
        {x^{t+1}_m, v^{t+1}_m} :=UPDATE PARTICLE(x^t_m, v^t_m, p^t_{b_m}, g^t_{b_m}, w, c_1, c_2)
        x^{t+1}_m :=ENFORCE CONSTRAINTS(x_m)
    end
end
RETURN A_t
```

this, the average Euclidean distance $\boldsymbol{d_o}$ from all goal positions $\boldsymbol{z_o}$ to the determined tip positions $\boldsymbol{ee}$ for each corresponding $\boldsymbol{x_m}$ is computed by:

$$\boldsymbol{d_o} = \frac{\sum_{m=1}^{P} ||\boldsymbol{z_o} - \boldsymbol{ee}(\boldsymbol{x_m})||_2}{P}. \tag{3}$$

The goal position $\boldsymbol{z_o}$ with $\min(\boldsymbol{d_o})$ defines the position which is closest to the initialized swarm and is therefore defined to be the first goal point $\boldsymbol{z_1}$ towards which the first tube set is being optimized, while other goal positions are also being considered such that their reachability also influences the optimization output.

DETERMINE PARTICLE COST: A particle's cost is defined by two objectives f_1 and f_2. Objective function f_1 defines the deviation from the manipulator's end effector position to the predefined goal point $\boldsymbol{z_1}$. Cost f_1 is determined by computing the Euclidean distance from the end effector position to the goal position. Objective function f_2 defines the number of reachable goal positions with one tube set. The number of reachable goal positions is determined by counting the number of reachable goal positions - neglecting $\boldsymbol{z_1}$- which are reachable by the tip positions $\boldsymbol{ee}$. A goal position is considered as reachable, if the Euclidean distance between $\boldsymbol{ee}$ and the goal position is $< 1\,\text{mm}$.

UPDATE ARCHIVE: The archive $\boldsymbol{A_t}$ serves as a storage for all *non-dominated* population members. Domination within a population is defined as follows: a particle $\boldsymbol{x_m}$ *strictly dominates* another particle $\boldsymbol{x_{m+1}}$ ($\boldsymbol{x_m} \prec \boldsymbol{x_{m+1}}$), if $f_j(\boldsymbol{x_m}) \leq f_j(\boldsymbol{x_{m+1}})$, $\forall j = 1...O$ for all j and $f_j(\boldsymbol{x_m}) < f_j(\boldsymbol{x_{m+1}})$ for some j. A particle $\boldsymbol{x_m}$ *weakly dominates* another particle $\boldsymbol{x_{m+1}}$ ($\boldsymbol{x_m} \preccurlyeq \boldsymbol{x_{m+1}}$), if $f_j(\boldsymbol{x_m}) \leq f_j(\boldsymbol{x_{m+1}})$ for all j. A non-dominated archive therefore means, that no particle is dominated by the other. Each non-dominated particle from the current population is added to $\boldsymbol{A_t}$. A particle is deleted from $\boldsymbol{A_t}$, if it is dominated by another particle within $\boldsymbol{A_t}$.

SELECT GUIDES: The personal best $\boldsymbol{p_{b_m}}$ value is determined according to [13]. If a particle $\boldsymbol{x_{m+1}}$ is not dominated by $\boldsymbol{p_{b_m}}$, then $\boldsymbol{p_{b_m}} = \boldsymbol{x_{m+1}}$. If the particle $\boldsymbol{x_{m+1}}$ is dominated by $\boldsymbol{p_{b_m}}$, $\boldsymbol{p_{b_m}}$ remains as the personal best value. The global best solution $\boldsymbol{g_{b_m}}$ effecting each particle is determined with the sigma-method, published in [14], which selects a particle from the archive $\boldsymbol{A_t}$ to be the global guide. To select the global guide from the archive, each particle is first assigned a σ- value as

$$\sigma = \frac{f_1^2 - f_2^2}{f_1^2 + f_2^2}. \tag{4}$$

If the two objectives f_1 and f_2 do not have the same range of values, σ is determined with the following equation:

$$\sigma = \frac{(K_2 \cdot f_1)^2 - (K_1 \cdot f_2)^2}{(K_2 \cdot f_1)^2 + (K_1 \cdot f_2)^2}, \tag{5}$$

where K_1 and K_2 are defined as the maximum achievable values within f_1 and f_2. The global best solution $\boldsymbol{g_{b_m}}$ for each particle is then determined by selecting the particle from the archive $\boldsymbol{A_t}$ as $\boldsymbol{g_{b_m}}$ which has the minimum σ-deviation to $\boldsymbol{x_m}$.

UPDATE PARTICLE: The particle's velocity and position are updated according to:

$$\boldsymbol{v_m^{t+1}} = w \cdot \boldsymbol{v_m^t} + c_1 \cdot r_1 \cdot (\boldsymbol{p_{b_m}^t} - \boldsymbol{x_m^t}) + c_2 \cdot r_2 \cdot (\boldsymbol{g_{b_m}^t} - \boldsymbol{x_m^t}), \tag{6}$$

$$\boldsymbol{x_m^{t+1}} = \boldsymbol{x_m^t} + \boldsymbol{v_m^{t+1}}, \tag{7}$$

with w being the inertia weight, c_1 and c_2 are constants controlling the influence of personal versus global best and r_1 and r_2 are randomly chosen in the range of $[0, 1]$. If $\boldsymbol{v_m^{t+1}}$ exceeds a prior defined maximum velocity $\boldsymbol{v_{max}}$, then $\boldsymbol{v_m^{t+1}} = \boldsymbol{v_{max}}$. The maximum velocity $\boldsymbol{v_{max}}$ is defined as 10 % of the range of values of each particle's dimension.

Enforce Constraints: To enforce constraints on the parameter space, particles exceeding the boundary are truncated at the boundary and their value is reflected by their boundary exceeding value, defined as upper $\boldsymbol{u_{b_p}}$ or lower boundary $\boldsymbol{l_{b_p}}$:

$$\boldsymbol{x_{m_p}^t} = \begin{cases} \boldsymbol{u_{b_p}} - (\boldsymbol{x_{m_p}^t} - \boldsymbol{u_{b_p}}) & , if \;\; \boldsymbol{x_{m_p}^t} > \boldsymbol{u_{b_p}} \\ \boldsymbol{l_{b_p}} + (\boldsymbol{l_{b_p}} - \boldsymbol{x_{m_p}^t}) & , if \;\; \boldsymbol{x_{m_p}^t} < \boldsymbol{l_{b_p}}. \end{cases} \tag{8}$$

with p being the number of parameters to be optimized. The upper $\boldsymbol{u_{b_p}}$ and lower boundaries $\boldsymbol{l_{b_p}}$ are chosen accordingly to the design constraints formulated in section 2.1.2.

Once the maximum number of generations G has been reached, the optimization ends. Then, we determine the number of reachable goal positions by the optimized tube set k and remove them from the set of reachable goal positions z_o. The algorithm starts over from the beginning, by only considering the remaining goal positions. This procedure continues until all goal positions are covered by a tube set. At the end of the optimization, the overall tube sets k to cover all goal positions are the output of the algorithm.

2.4 Evaluation

The particle swarm algorithm optimizes the tube parameters $\boldsymbol{x_m}$ for k minimum number of tube sets for three patient datasets, as illustrated in Figure 4. We determine the minimum number of tube sets required to provide each of the three kidneys, where each of the kidneys is defined by 5 goal positions. Further, the minimum number of tube sets required to provide all three kidneys is determined. We define the following parameters empirically: the generation size is $G = 500$, the number of particles $P = 20$, the inertia $w = 0.9$ and $c_1 = c_2 = 2$.

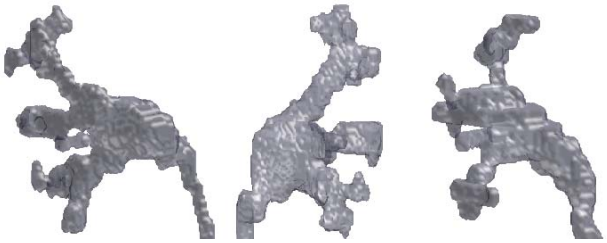

Figure 4: Three patient kidneys. Two of them are right-side kidneys (Patient 1 and 3), one of them is a left-side kidney (Patient 2).

3 Results

The optimization resulted in 2 successively used tube sets for Patient 1 and 3. Patient 2 requires the use of 3 successively used tube sets. To provide all 3 patient datasets, 5 different tube sets were optimized to cover all kidneys. Figure 5 illustrates 10000 configuration samples for each of the 2 optimized tube sets for patient 1 marked in blue and green respectively. The results were computed on the cluster system at the Leibniz Universität Hannover, Germany and implemented in Matlab.

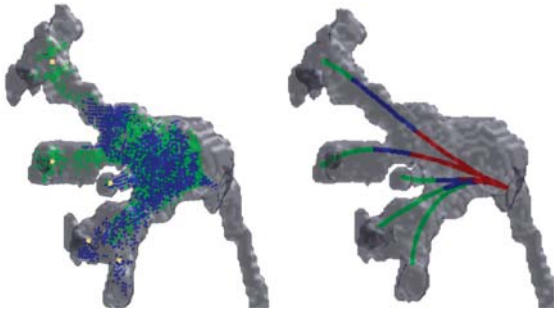

Figure 5: 10000 configuration samples for each of the 2 optimized tube sets for patient 1 marked as blue and green dots (left). Goal positions are marked as yellow dots. Example manipulator configurations reaching the goal positions (right).

4 Conclusion

We presented a new concept and an initial study for transurethral kidney procedures using tubular manipulators. Design constraints were considered according to three real patient datasets. A multiobjective particle swarm optimization was proposed, which considers multiple objectives in contrast to existing optimization algorithms for tubular continuum manipulators. Results have shown, that the use of two to three successively used tube sets can provide optimal positioning of the manipulator within the kidney of one patient. We foresee the exchange of tubes during the intervention to be quick and easy as this resembles current intraoperative practice. We believe, that this concept has the potential to greatly increase the transurethral manipulability within the kidney in comparison to manually operated ureterorenoscopes. Further, robustness and handling could be improved and the use of guide wires omitted. This might allow less proficient urologists to perform these challenging interventions. In the future, we plan to evaluate further patient kidney datasets to determine the overall number of sets of tubes necessary to provide the majority of patients, build a physical prototype, and conduct experiments.

5 Acknowledgment

This work is funded by the German Research Foundation (DFG) under award BU 2935/1-1. We thank T.-D. Nguyen for images and illustrations.

References

[1] A. Breda, O. Ogunyemi, J. T. Leppert, and P. G. Schulam, "Flexible Ureteroscopy and Laser Lithotripsy for Multiple Unilateral Intrarenal Stones," *European Urology*, vol. 55, no. 5, pp. 1190–1197, 2009.

[2] P. Geavlete, D. Georgescu, G. Nita, V. Mirciulescu, and V. Cauni, "Complications of 2735 Retrograde Semirigid Ureteroscopy Procedures: A Single-Center Experience," *Journal of Endourology*, vol. 20, no. 3, pp. 179–185, 2006.

[3] J. Burgner-Kahrs, D. C. Rucker, and H. Choset, "Continuum Robots for Medical Applications: A Survey," *IEEE Transactions on Robotics*, vol. 31, no. 6, pp. 1261–1280, 2015.

[4] R. J. Hendrick, S. D. Herrell, and R. J. Webster III, "A Multi-Arm Hand-Held Robotic System for Transurethral Laser Prostate Surgery," *IEEE International Conference on Robotics and Automation*, pp. 2850–2855, 2014.

[5] C. Bedell, J. Lock, A. H. Gosline, and P. E. Dupont, "Design Optimization of Concentric Tube Robots Based on Task and Anatomical Constraints," in *IEEE International Conference on Robotics and Automation*, pp. 398–403, 2012.

[6] J. Burgner, H. B. Gilbert, and R. J. Webster III, "On the computational design of concentric tube robots: Incorporating volume-based objectives," in *IEEE International Conference on Robotics and Automation*, pp. 1193–1198, 2013.

[7] C. Bergeles, A. H. Gosline, N. V. Vasilyev, P. J. Codd, P. J. del Nido, and P. E. Dupont, "Concentric Tube Robot Design and Optimization Based on Task and Anatomical Constraints," *IEEE Transactions on Robotics*, vol. 31, no. 1, pp. 67–84, 2015.

[8] C. Baykal, L. G. Torres, and R. Alterovitz, "Optimizing Design Parameters for Sets of Concentric Tube Robots using Sampling-based Motion Planning," in *IEEE International Conference on Intelligent Robots and Systems*, pp. 4381–4387, 2015.

[9] D. C. Rucker, R. J. Webster III, G. S. Chirikjian, and N. J. Cowan, "Equilibrium conformations of concentric-tube continuum robots," *International Journal of Robotics Research*, vol. 56, no. 10, pp. 1263–1280, 2010.

[10] T. Lee, R. Kashyap, and C. Chu, "Building skeleton models via 3-d medial surface/axis thinning algorithms," *Graphical Models and Image Processing*, vol. 56, no. 6, pp. 462–478, 1994.

[11] J. Kennedy and R. Eberhart, "Particle swarm optimization," in *IEEE International Conference on Neural Networks*, pp. 1942–1948, 1995.

[12] J. Moore and R. Chapman, "Application of particle swarm to multiobjective optimization," *Department of Computer Science and Software Engineering Department, Auburn University*, pp. 1–4, 1999.

[13] J. Branke and S. Mostaghim, *About Selecting the Personal Best in Multi-Objective Particle Swarm Optimization*, pp. 523–532. Berlin, Heidelberg: Springer Berlin Heidelberg, 2006.

[14] S. Mostaghim and J. Teich, "Strategies for Finding Good Local Guides in Multiobjective Particle Swarm Optimization (MOPSO)," in *IEEE Swarm Intelligence Symposium*, pp. 26–33, 2003.